Development of smart molecularly imprinted tetrahedral amorphous carbon thin films for in vitro dopamine sensing

Journal of Electroanalytical Chemistry 976 (2025) 118742

Contents lists available at ScienceDirect

Journal of Electroanalytical Chemistry

journal homepage: www.elsevier.com/locate/jelechem

Development of smart molecularly imprinted tetrahedral amorphous carbon thin films for *in vitro* dopamine sensing

Giorgia Rinaldi [a], Khadijeh Nekoueian [b,*], Jarkko Etula [c,d], Tomi Laurila [b,d,*]

[a] Department of Applied Science and Technology (DISAT), Politecnico di Torino, Corso Duca degli Abruzzi 24, 10129 Torino, Italy
[b] Department of Electrical Engineering and Automation, School of Electrical Engineering, Aalto University, P.O. Box 13500, 00076 Aalto, Finland
[c] Canatu Oy, Tiilenlyöjänkuja 9, Vantaa 01720, Finland
[d] Department of Chemistry and Materials Science, School of Chemical Engineering, Aalto University, PO Box 16100, 00076 Aalto, Finland

ARTICLE INFO

Keywords:
Tetrahedral amorphous carbon thin films
Electrochemical molecular Imprinting
Electrochemical characterization
Dopamine detection

ABSTRACT

This study investigates how varying the thickness of tetrahedral amorphous carbon (ta-C) thin films and incorporating a titanium adhesion layer influences the structural and electrochemical properties of molecularly imprinted ta-C thin film-based sensing platforms, aiming to develop a molecularly imprinted ta-C electrochemical sensor for dopamine (DA) detection with physiologically relevant sensitivity. This electrochemical sensing platform was designed by integrating ta-C with molecularly imprinted polymers (MIPs). The process involved depositing a ta-C thin film onto boron-doped p-type silicon wafers through a filtered cathodic vacuum arc (FCVA) system. Subsequently, the ta-C sensing platforms were electrochemically coated with the MIP layer (DA-imprinted polypyrrole). We evaluated three configurations: (i) a 15 nm ta-C layer, (ii) a 7 nm ta-C layer with a 20 nm titanium adhesion layer, and (iii) a 15 nm ta-C layer with a 20 nm titanium adhesion layer. Comprehensive structural and electrochemical characterization was performed to understand how these modifications affect sensor performance. The optimized MIP/ta-C sensor demonstrated a sensitivity of 0.16 μA μM^{-1} cm^{-2} and a limit of detection (LOD) of 48.6 nM, suitable for detecting DA at physiological levels. Leveraging the synergistic effects of ta-C coatings and molecular imprinting, as well as its compatibility with common complementary metal–oxide–semiconductor (CMOS) processes underlines its potential for integration into microanalytical systems, paving the way for miniaturized and high-throughput sensing platforms.

1. Introduction

Neurotransmitters (NTs), specifically DA, are pivotal in regulating brain functions since any disruption in their activity can precipitate neurological disorders such as Parkinson's disease, schizophrenia, and Alzheimer's disease. Different approaches, such as chromatography and mass spectrometry, have been developed to detect NTs accurately. These methods are costly, time-consuming, and require complex sample preparation [1], whereas electrochemical methods offer a cost-effective, portable, rapid, and sensitive detection solution [2].

The *in vitro* determination of NTs within their physiologically relevant concentration range of 25–1000 nM demands a specific sensing platform with several key properties, such as (i) the ability to detect NTs quickly, (ii) long-term stability to mitigate electrode fouling in complex matrices, ensuring reliable and accurate measurements over extended periods, and (iii) the capability to detect NTs in the presence of potential interferents present in real samples, such as ascorbic acid (AA) [2–4]. However, the studies conducted by Rantataro et al. in our group demonstrate that AA does not consistently impede the electrochemical detection of DA in a cell culture medium [5]. Notably, AA undergoes rapid decay in cell culture medium, with a half-life of 2.1 h, resulting in a 93.0 % decrease in concentration within 8 h and a 99.7 % decrease within 18 h. Consequently, AA becomes undetectable by electrodes over time, allowing for effective monitoring of NTs concentrations [5].

Carbon nanomaterials, owing to their high electron transfer rates, hold promise for improving sensor performance [6,7]. Amorphous carbon is a non-crystalline material characterized by a high number of sp^3 bonds [8]. Compared to its bulk form, a 2D ta-C film is characterized by a high sp^2 fraction, which allows for fast electron transfer and higher conductivity [8,9]. Amorphous carbon is also characterized by a low background current, a wide potential window [10,11], and compatibility with CMOS processes [12]. Moreover, the biocompatibility of

* Corresponding authors.
E-mail addresses: Khadijeh.Nekoueian@Aalto.Fi (K. Nekoueian), Tomi.Laurila@Aalto.Fi (T. Laurila).

https://doi.org/10.1016/j.jelechem.2024.118742
Received 10 September 2024; Received in revised form 18 October 2024; Accepted 24 October 2024
Available online 26 October 2024

tetrahedral amorphous carbon (ta-C) has been extensively validated in our group [9–12], demonstrating not only cell adhesion but also its potential antifouling properties, which are crucial for sensor longevity and performance [13], facilitating further application in cell-cultured-based sensors on CMOS [13].

The distinct surface properties of ta-C thin films offer a versatile platform for tailoring surfaces to meet specific application needs. This characteristic is particularly valuable in electrochemical applications, including those utilizing surface-modified ta-C coatings for DA sensing [14,15]. Molecular imprinting represents another strategy to enhance sensor performance. It involves the creation of recognition sites tailored to the target analyte, improving sensor sensitivity while maintaining low costs [1,16]. This technique consists of the formation of a polymeric film in the presence of a template molecule. After template removal, nano-sized cavities are left behind, acting as artificial receptors, and selectively rebinding to the target analyte [3,17]. Molecular imprinting can also counteract the electrode surface's passivation [3,16]. In the present study, polypyrrole (PPy), a biocompatible conducting polymer (CP), has been used to molecularly imprint DA molecules on the surface of ta-C [18]. PPy is characterized by low cost and superior electrochemical properties, such as a wide dynamic range and a low detection limit [18,19]. In addition, PPy can be electrochemically imprinted at room temperature, preventing denaturation and conformational change [19]. Finally, PPy also ensures easy template removal and rebinding of the target molecule [17,19].

The objective of this study is to develop a sensitive MIP-based ta-C sensor (MIP/ta-C) for the detection of DA with physiologically relevant sensitivity in a phosphate-buffered saline (PBS) solution at physiologically relevant pH 7.4, with future applications envisioned *in vitro* testing using cell culture media. The process involved depositing a ta-C thin film onto boron-doped p-type silicon wafers with a nickel catalyst and Ti adhesion layers through a filtered cathodic vacuum arc (FCVA) system based on previous studies in our research group [20–23]. Subsequently, the ta-C sensing platforms with various thicknesses and structures were electrochemically coated with the optimal MIP layer (DA imprinted polypyrrole). Multiple configurations were evaluated to identify the optimal sensing platform for DA detection, focusing on ta-C and MIP/ta-C architectures. These included (i) a 7 nm ta-C layer and (ii) a 15 nm ta-C layer in the presence or absence of a 20 nm titanium adhesion interlayer between the silicon substrate and ta-C thin films. Additionally, key parameters for the electrochemical formation of the MIP layer and the detection of DA were optimized to enhance the sensitivity of the MIP/ta-C architecture. The factors studied include (i) the molar ratio of functional monomers to template molecules, and (ii) the pH of the imprinting electrolyte, as well as (iii) the thickness of the MIP layer, (iv) the scan rate and number of CV cycles during polymerization, and (v) the incubation time.

Then, the physicochemical and electrochemical properties of these ta-C and MIP/ta-C electrodes were studied to assess structural variations and correlate them with electrochemical performance. The study investigated the surface morphology and topography of ta-C and MIP/ta-C samples using scanning electron microscopy and atomic force microscopy techniques. These methods allowed for a detailed evaluation of surface roughness for both the bare ta-C and the MIP/ta-C samples. Raman spectroscopy was employed to analyze the structure of the ta-C and MIP/ta-C, focusing on the I_D/I_G ratio, which is indicative of the sp^2 (graphitic) to sp^3 (diamond-like) carbon content in the films. The electrochemical properties were evaluated using an outer-sphere redox probe, $Ru(NH_3)_6^{3+/2+}$, and an inner-sphere redox probe, DA, which also served as a target template molecule. These studies, along with the electrochemical characterization of the samples, contributed to the design of a high-performance MIP/ta-C sensing platform.

Our previous studies revealed that the I_D/I_G ratio decreases as the film thickness increases from 7 to 15 nm [15,23]. This decrease indicates a significant reduction in sp^2 content, suggesting that the films become more diamond-like (sp^3-rich) as they grow thicker [15,23]. The reduced sp^2 content and improved structural characteristics likely enhance the sensitivity of the MIP/ta-C sensor compared to ta-C, making it a promising candidate for advanced sensing applications. A comprehensive study on the electrochemical and physicochemical characterization of ta-C is available in our previous publication [7,15,23], offering additional context to our current research [8,15,17]. Additionally, the system exhibits potential compatibility with common complementary metal oxide semiconductor (CMOS) processes, enabling its integration into microelectrode arrays (MEAs) for future *in vitro* studies.

2. Materials and methods

2.1. Chemicals and instruments

Sodium chloride, potassium chloride, disodium hydrogen phosphate and potassium hydrogen phosphate were purchased from Emsure. DA hydrochloride and Hexaammineruthenium (III) were purchased from Sigma-Aldrich. Lastly, pyrrole 98 % was purchased from Alfa Aesar. All solutions were based on PBS solution and KCl solution, which were prepared with deionized water (DIW).

All the experiments were carried out at room temperature inside a Faraday cage. DA is prone to oxidation, leading to its self-polymerization into a melanin-like substance called polydopamine [24]. This polymerization mainly occurs in alkaline conditions with oxygen present [24]. As the reaction time increases, more polydopamine forms, causing the DA solution to darken. To prevent polydopamine formation, the electropolymerization solution was degassed for 1 h. This step is crucial, as oxygen accelerates the formation of polydopamine [25]. Both our experiments and findings from Nekoueian et al. [17] suggest that degassing the electropolymerization solution and DA solutions for 1 h effectively prevents polydopamine formation [17], and leads to clear DA solutions for measurements.

The potentiostats used for electrochemical measurements were Gamry Instruments Reference 600 + Potentiostat/Galvanostat/ZRA or Gamry Instruments Reference 600 Potentiostat/Galvanostat/ZRA. The setup was a three-electrode system. The reference electrode for the electrochemical studies was an Ag/AgCl, while an Ag wire was used for the electrodeposition step. The counter electrode considered was a Pt wire for all the measurements. The pH of the PBS solution was adjusted with the pH/mV/°C meter, pHenomenal® pH 1100 L. Electrochemical experiments were conducted by using CV and differential pulse voltammetry (DPV) in 0.1 M PBS solutions with variable concentrations of DA with a standard three-electrode system. The Randles equivalent circuit was employed for fitting the Nyquist plots obtained from electrochemical impedance spectroscopy (EIS) studies in 5 mM $Ru(NH_3)_6^{2+/3+}$ in 1 M KCl solution at ta-C-based electrodes. The Randles equivalent circuit consists of a solution resistance (R_s) in series with a parallel configuration containing a charge transfer resistance (R_{ct}), a Warburg element (W), and a constant phase element (CPE), which replaces the conventional double-layer capacitance (C_{dl}). The R_{ct} comprises two components: (i) electron transfer to the electrode surface and (ii) electron transport through the film [21]. The parameter α measures the deviation of the CPE's characteristics from those of an ideal capacitor (where α = 1). The standard heterogeneous constant $k^{0'}$ at formal potential was evaluated by using Eq. (1) [26] and R_{ct}. The R_{ct} was calculated by Gamry Echem Analyst software [7].

$$k^{0'} = RT \cdot \left(F^2 A R_{ct} \left(c_O^b\right)^{\alpha} \left(c_R^b\right)^{1-\alpha} \right)^{-1} \quad (1)$$

here, 'R' signifies the gas constant, 'T' denotes the temperature, 'F' represents the Faraday constant, 'A' denotes the geometrical area of the electrode (with A = 0.07 cm2), 'c' indicates the concentration Ru

$(NH_3)_6^{2+/3+}$, and 'α' represents the transfer coefficient (with α = 0.5 assumed). The subscripts 'O' and 'R' denote the oxidized and reduced species, respectively, while the superscript 'b' denotes the bulk concentration [7,26].

The scanning electrode microscopy (SEM) images were taken with the Zeiss Sigma VP (Entry-level SEM) – NMC. The atomic force microscopy (AFM) 3D surface maps were taken with a Bruker Dimension Icon AFM. A WITec alpha300 RA + Raman Spectroscope with a laser excitation length of 532 nm using a 50X objective lens was used to acquire the Raman spectra.

2.2. Preparation of the ta-C

The ta-C thin films with various thicknesses (7 and 15 nm) were deposited onto (i) titanium adhesion layers atop boron-doped p-type silicon wafers and (ii) boron-doped p-type silicon wafers without titanium adhesion layer based on previous studies in our group [21,27]. Before deposition, the samples underwent standard cleaning procedures. The titanium adhesion layers, 20 nm thick, were deposited using direct-current magnetron sputtering (DC-MS), while ta-C films were deposited utilizing a filtered cathodic vacuum arc (FCVA) system. Both deposition systems were kept within the same vacuum chamber equipped with appropriate pumps. The magnetron sputtering system utilized a circular Ti target and specific deposition parameters, including discharge power, total pressure, Ar gas flow rate, and deposition times. The FCVA system, equipped with a magnetic filter to reduce contamination, employed graphite cathodes in a dual cathode configuration. During deposition, the samples were rotated to ensure uniform film deposition [21].

2.3. Preparation of the MIP/ta-C electrodes

The electrodes have been assembled using copper as a substrate and polytetrafluoroethylene (PTFE) to fix the ta-C-modified silicon wafer to the substrate and to outline the active surface area 0.07 mm^2, as shown in Scheme 1S. The ta-C samples were used to prepare the working electrodes for the sensing system. In this regard, their backside was scratched using a diamond pen first and a copper palette. After that, the sample was connected to a copper FR4-PBB body with a protective coverage of PTFE tape with a 3 mm diameter hole (applied electrode surface area) used to sandwich the sample and copper sheet. The electrochemical molecular imprinting is performed under optimized conditions in a freshly prepared degassed 1 M PBS solution containing both the functional monomer (pyrrole) and the target analyte (DA) by using CV. Fig. 1A represents the cyclic voltammograms referred to the electrochemical imprinting process for the MIP layer on ta-C, which exhibits decreasing peak current at each cycle, proving the deposition of the polymeric layer.

The non-imprinted polymer (NIP) modified electrodes, namely NIP/ta-C electrodes, were prepared without the presence of the template molecule in the electrodeposition step. After the imprinting process, the electrodes undergo a two-step washing procedure meant to remove the template molecules from the imprinting sites. The first step consists of placing the electrodes into a solution of ethanol and DIW (1:1 V/V) for 15 min to remove the unreacted monomers from the electrode surface. The second step involves the electrochemical template removal of the MIP/ta-C electrodes by running several CV cycles in PBS at pH 7.4, as shown in Fig. 1B. After the disappearance of DA redox signals, the MIP/ta-C electrodes are tested in PBS by DPV. Once the DPV does not show any peak for DA anymore, the electrodes are ready to use [17].

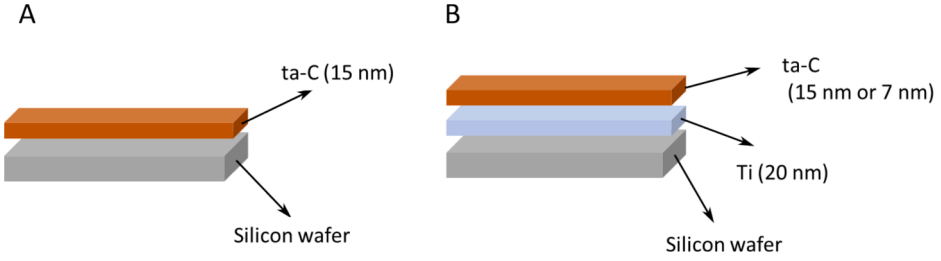

Scheme 1. Schematics of different ta-C samples (A) coating with a 15 nm thick ta-C layer (B) coating with a 20 nm titanium adhesion layer and a variable thickness of ta-C (7 nm and 15 nm).

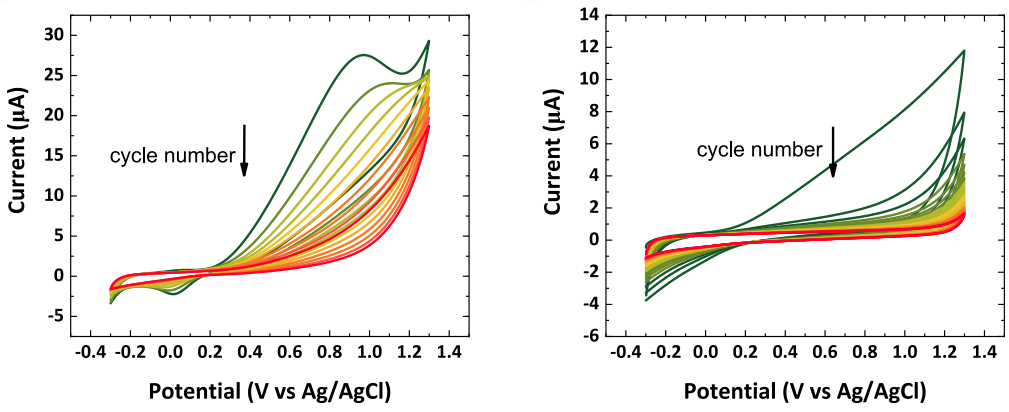

Fig. 1. (A) CVs of the electrochemical imprinting, (B) CVs of electrochemical template removal at MIP/ta-C in PBS.

3. Results and discussion

3.1. Structural characterization

SEM and AFM methods explored the surface morphology and topography of both bare ta-C and MIP/ta-C samples. Fig. 2A and 2B display SEM images of ta-C and MIP/ta-C samples, while Fig. 3A, 3B, and Fig. S1 showcase the AFM surface topography maps of ta-C and MIP/ta-C samples. Although the imprinted sites are not visible in SEM images, clear evidence of the electropolymerization of a PPy layer over the ta-C surface is observed. AFM surface topography maps were then employed to evaluate the surface roughness (R_q) of ta-C and MIP/ta-C samples, as presented in Table 1. The results in Table 1 indicate a significant enhancement in surface roughness due to the surface modification of ta-C with MIP compared to the bare substrate. Additionally, it is noteworthy that MIP modification notably increases roughness for both silicon and ta-C substrates.

Raman spectroscopy was used to analyze the structure of bare ta-C and PPy/ta-C films. The spectra, shown in Fig. 3C, display a D band around 1360 cm^{-1} and a G band around 1550 cm^{-1}, which correspond to the sp^2 content in the ta-C film [15,21,23]. These peaks diminish when the PPy layer is electrodeposited onto the ta-C film, indicating changes in the sp^2 fraction. These findings for ta-C are consistent with results from our previous studies [21].

For ta-C thin films, the Raman spectra were processed by subtracting the background and normalizing the silicon (Si) peak. The I_D/I_G ratio, which represents the proportion of disordered (sp^2) carbon to graphitic (sp^3) carbon, is crucial because it relates to key material properties such as mass density and the mobility gap [15,21,27,28]. Previous studies in our research group demonstrated that as the ta-C film thickness increased from 7 nm to 15 nm, the I_D/I_G ratio decreased from 0.56 ± 0.01 to 0.47 ± 0.02 [21], indicating a significant reduction in sp^2 content [21,29]. This suggests that thicker films have a more graphitic and less disordered structure [15,21,27]. These findings, along with the films' electrochemical properties, offer valuable insights for designing a high-performance MIP/ta-C sensing platform. The reduced sp^2 content in thicker films likely enhances their sensing capabilities, making them more suitable for advanced sensor applications.

Table 1
R_q measured by AFM for plain silicon (Si), MIP/Si, plain ta-C, and MIP/ta-C samples in the 5 μm × 5 μm region on the sample.

	Si	MIP/Si	ta-C	MIP/ta-C
R_q (nm)	0.35	1.38	0.78	1.11

3.2. Electrochemical characterization

The electrochemical properties of ta-C, NIP/ta-C, and MIP/ta-C electrodes were investigated in 5 mM $Ru(NH_3)_6^{3+/2+}$, 1 M KCl as an outer sphere redox (OSR) probe by using CV (Fig. 4A) and EIS (Fig. 4B) methods. It is important to highlight that the results obtained using the OSR probe are independent of any chemical interaction with the electrode surface and correspond to the electronic structure of the electrode material [7]. Comparing the onset potential of $Ru(NH_3)_6^{3+/2+}$ oxidation at different electrodes can provide insights into their electrocatalytic activity. Results obtained from the CVs tabulated in Table 2 indicate that the onset anodic potentials of ta-C, NIP/ta-C, and MIP/ta-C electrodes

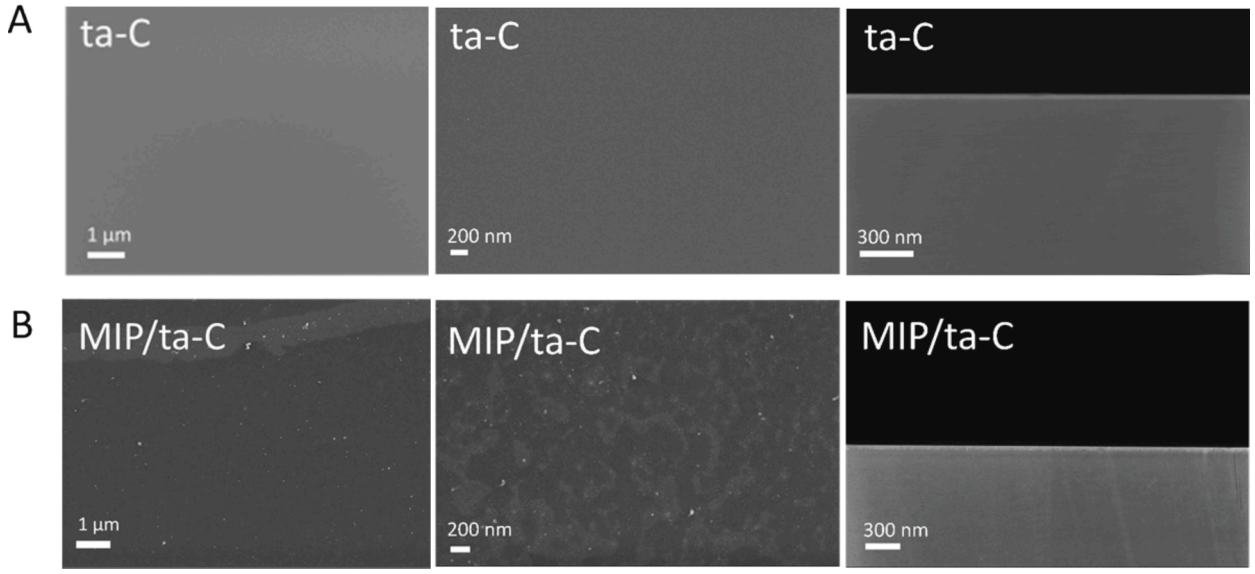

Fig. 2. Front and cross-sectional SEM images of (A) ta-C samples and (B) MIP/ta-C samples.

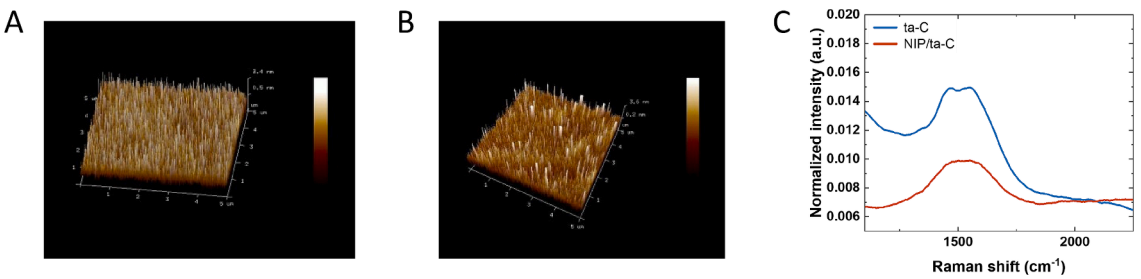

Fig. 3. AFM surface topography maps in the 5 μm × 5 μm region of (A) ta-C sample and (B) MIP/ta-C sample, along with (C) Raman spectra of bare ta-C and PPy/ta-C. The Raman spectra were obtained using a laser excitation wavelength of 532 nm and a 50X objective lens.

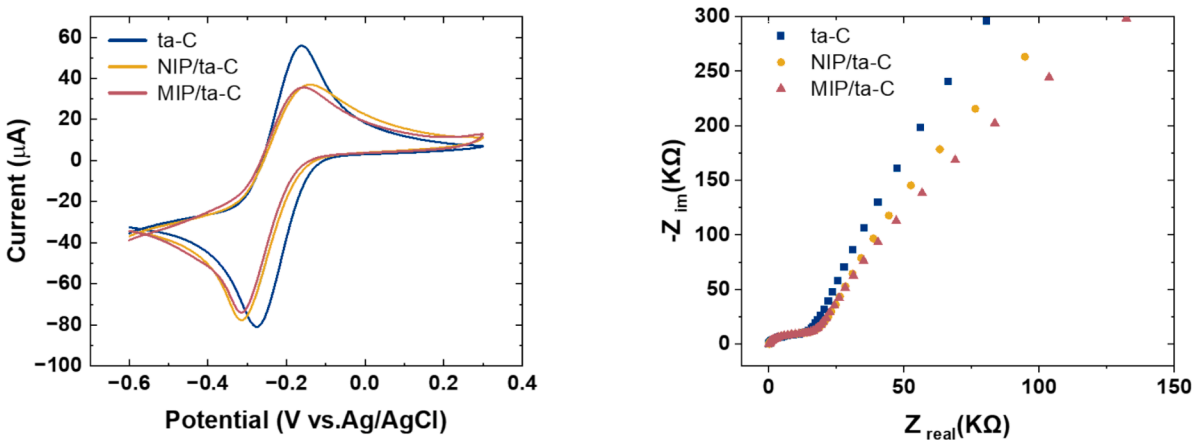

Fig. 4. (A) CVs and (B) Nyquist plots of ta-C, NIP/ta-C and MIP/ta-C electrodes in 5 mM $Ru(NH_3)_6^{3+/2+}$, 1 M KCl with the Randles equivalent circuits used for fitting. The scan rate was 100 mVs^{-1}.

Table 2
The comparison of the results obtained from the CVs for ta-C, NIP/ta-C, and MIP/ta-C electrodes in 5 mM $Ru(NH_3)_6^{2+/3+}$ in 1 M KCl solution (N = 3).

Sample	I_{pa} (μA)	I_{pc} (μA)	I_{pa}/I_{pc}	E_{pa} (mV)	E_{pc} (mV)	ΔE_p (mV)	E_{onset} (mV)
NIP/ta-C	46.5 ± 0.64	−61.3 ± 0.41	0.77 ± 0.05	−141 ± 0.72	−313 ± 0.13	171	−297 ± 0.24
MIP/ta-C	45.3 ± 0.40	−56.5 ± 0.25	0.76 ± 0.04	−154 ± 0.07	−315 ± 0.25	159	−306 ± 0.21
ta-C	73.1 ± 0.09	−71.8 ± 0.33	1.02 ± 0.00	−156 ± 0.40	−279 ± 0.41	123	−292 ± 0.15

Table 3
Comparison of the parameters obtained from EIS for ta-C, NIP/ta-C, and MIP/ta-C electrodes in the presence of 5 mM $Ru(NH_3)_6^{2+/3+}$ in 1 M KCl solution. The ta-C samples used were without Ti interlayer. More detailed information is available in previous studies [21].

Sample type	R_s (Ω)	R_{ct} (Ω)	k^0 (cm/s)
NIP/ta-C	135	20.570	0.00073
MIP/ta-C	136	20.140	0.00074
ta-C	134	16.860	0.00089

are similar to each other. This suggests all electrodes have comparable electrocatalytic activities for the OSR probe used, namely Ru $(NH_3)_6^{3+/2+}$. It may also suggest that the reaction kinetics at these electrodes are governed by similar mechanisms. These findings from CV support those from EIS, as depicted in Fig. 4B. The Nyquist plot from EIS measurements reveals a small semicircle associated with R_{ct} in the high-frequency range for the ta-C, NIP/ta-C and MIP/ta-C electrodes. In the low-frequency range, diffusion dominates the response, as indicated by a linear trend. The magnitude of this semicircle does not change significantly with the formation of PPy on ta-C (Fig. 4B). After fitting the EIS curves to the Randles equivalent circuit, the electron transfer resistance R_{ct} and the R_s were evaluated, as shown in Table 3. The R_s was constant for all samples, as the same solution was used in the studies. Furthermore, the k^0 was calculated to study the kinetics of a redox couple, expressing the velocity needed for the system to reach the equilibrium state. As the k^0 is higher, the equilibrium is reached faster [20]. There is no significant difference among calculated R_{ct} for the ta-C, MIP/ta-C electrode and NIP/ta-C, which aligns with expectations drawn from the CV measurements, where there were minor increases in ΔE_p values (Table 2) observed with the incorporation of MIP and NIP layers. Notably, k^0 exhibited a slight decrease, as shown in Table 3. Under these circumstances, we assume that the density of states at the electrode's surface remained constant in the presence of OSR. The small differences in reaction kinetics of these redox couples should be related only to the varying electrical properties of the ta-C film due to the formation of the PPy layer as supported by Raman spectra (Fig. 3C).

The electrochemical performance of ta-C, NIP/ta-C, and MIP/ta-C electrodes was examined using DA (the template molecule) at a concentration of 10.0 μM in PBS at pH 7.4. It is crucial to recognize that DA acts as an inner sphere redox probe (ISR), directly engaging in the electrode's redox reactions and being heavily affected by the surface chemistry of the electrode [7]. Consequently, there is no correlation between the electrochemical results of the OSR probe and the electrochemical performance of electrodes (MIP, NIP, and ta-C) in the presence of DA (the template molecules), which also acts as an ISR probe. Fig. 5A illustrates the impact of surface modifications of ta-C with MIP and NIP layers on the redox behavior of DA using CV. The creation of molecularly imprinted sites on the ta-C electrode facilitated specific interactions with DA molecules, resulting in a heightened response signal compared to both the NIP/ta-C and the bare ta-C electrode. The absence of any DA oxidation signal in the PBS solution before DA measurements confirmed the complete removal of template molecules (DA) from the MIP/ta-C sensing platform (Fig. 5B and Fig. S2). Consequently, the observed signal is not attributed to any trapped or unremoved DA molecules (template) within the MIP layer, confirming the successful formation of the MIP layer for DA sensing.

3.3. Optimization of the experimental conditions

The effects of several key parameters were studied and optimized to develop a sensitive MIP/ta-C architecture for DA sensing. These parameters include (i) the thickness of the ta-C layer and the presence of a titanium adhesion layer, (ii) the molar ratio of functional monomers to template molecules in the imprinting solution, (iii) the pH of the imprinting solution, (iv) the thickness of the MIP layer, and (v) the incubation time. The optimization results are detailed in Table 4.

3.3.1. Effect of the thickness of the ta-C layer and the presence of a titanium adhesion layer on the performance of MIP/ta-C electrodes

The effect of the thickness of the ta-C layer and the presence of a titanium adhesion layer on the performance of MIP/ta-C electrodes in 10.0 μM DA solution in PBS pH 7.4 was studied and is shown in Scheme 1. Different electrodes were prepared using (i) 15 nm ta-C, (ii) 7 nm ta-C with a 20 nm titanium adhesion layer, and (iii) 15 nm ta-C with a 20 nm

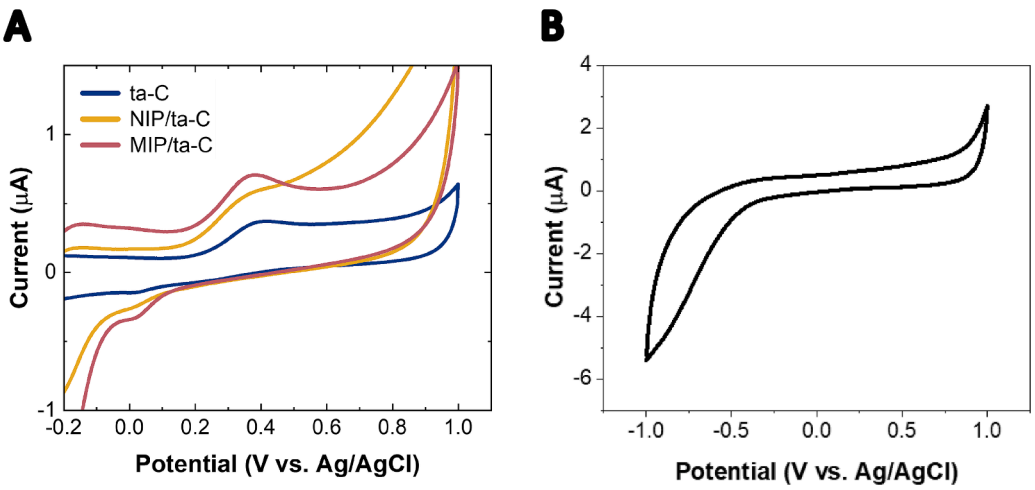

Fig. 5. (A) CVs of ta-C, NIP/ta-C and MIP/ta-C electrodes in 10.0 μM DA in PBS at pH 7.4, and (B) CVs of MIP/ta-C electrodes in PBS at pH 7.4. The scan rate was 100 mVs^{-1}.

Table 4
Optimized parameters at MIP/ta-C electrode for detection of DA.

Parameter optimized	Target	Optimized values
Monomer-to-template ratio	Increase of active recognition sites	1:1
MIP layer thickness	Accessibility of recognition sites, and ease of template removal step	Number of CVs: 10 Scan rate: 100 mV/s
Incubation time	Increase the sensitivity of the MIP/ta-C sensor	10 min

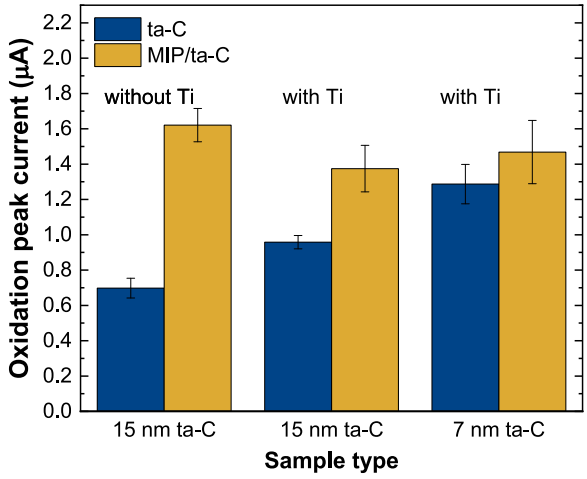

Fig. 6. Effect of the thickness of the ta-C layer and the presence of a titanium adhesion layer in DA detection performance of ta-C and MIP/ta-C.

titanium adhesion layer. These electrodes were examined for the detection of 10.0 μM DA in a PBS (pH 7.4) solution.

Fig. 6 shows the performance of the different ta-C electrodes before and after modification with the MIP layer. Different electrochemical performances observed for each ta-C sensing architecture correlated with the thickness of the ta-C layer. A thinner ta-C coating (7 nm) is characterized by a higher fraction of sp^2 [18], which results in better electron transfer [15,21,27]. The increase in the ta-C film thickness probably resulted in a reduction in the volume of the sp^2 fraction and an enlargement of the mobility gap, causing a decrease in the average current flow through the film [21]. Moreover, the impact of a titanium interlayer between the substrate and the ta-C film was investigated. The results indicate that the incorporation of Ti decreases charge transfer resistance and enhances double-layer capacitance, thereby accelerating reaction kinetics [21]. Furthermore, the 15 nm ta-C layer with the titanium adhesion layer behaves worse than the 7 nm ta-C with the titanium adhesion layer due to the increased ta-C thickness (Fig. 6).

The same study was conducted with MIP/ta-C electrodes. The DA interaction with the MIP/ta-C sensing platform remains approximately constant for all MIP/ta-C electrodes, regardless of ta-C film thickness and the presence of a titanium adhesion layer, as shown in Fig. 6 These results suggest that the interaction between MIP/ta-C films and DA is restricted to the surface, causing the recognition to be independent of the bulk properties of the films. Consequently, the similar performance achieved for different samples might stem from the presence of a similar amount of DA recognition sites on different MIP/ta-C films. In this light, surface modification substantially enhances the performance of the devices relative to their unmodified counterparts, making them more suitable for DA sensing. The optimal sensing substrate was determined to be the 15 nm ta-C sample without the titanium adhesion layer. Thus, all further measurements were conducted using this configuration (15 nm ta-C). The physicochemical and electrochemical properties of the 7 nm and 15 nm ta-C samples were compared and presented in Fig. S3 and Tables S1–S3. These Supplementary materials provide a detailed analysis of the structural, chemical, and electrochemical differences between the two ta-C thicknesses.

3.3.2. Effect of the molar ratio of functional monomers to template molecules in the imprinting solution

The effect of the template molecule (DA) to functional monomer (pyrrole) concentration ratio has been studied considering the performance of the DA-imprinted PPy electrode towards DA detection. The template concentration has been kept constant at 2 mM while the concentration of the functional monomer varied (the molar ratios were 1:1, 1:3, 1:5, 1:7, and 1:9). Peak current decreased at higher ratios of pyrrole in the solution due to the decrease in the number of template molecules involved in the formation of recognition sites necessary for sensing. Consequently, the ratio providing the best results was identified to be 1:1, as shown in Fig. 7A.

3.3.3. Effect of the pH of the imprinting solution

The performance of the MIP/ta-C sensor for DA detection was

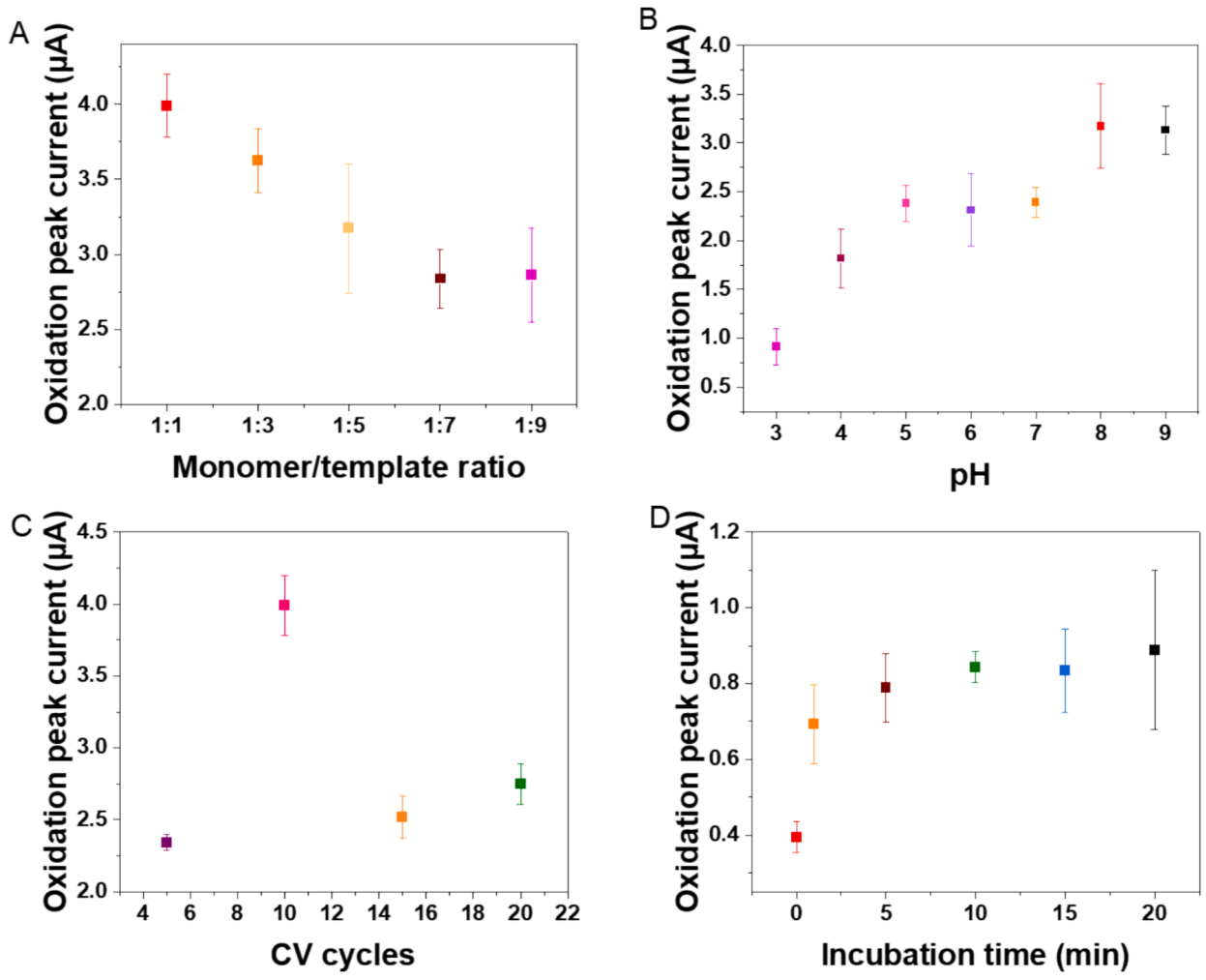

Fig. 7. Optimized parameters for detecting DA at the MIP/ta-C electrode included: (A) Varying ratios of functional monomer (pyrrole) to template molecules (DA) at 1:1, 1:3, 1:5, 1:7, and 1:9, (B) electrodeposition pH levels ranging from 3 to 9, (C) different numbers of CV cycles, specifically 5, 10, 15, and 20, and (D) incubation times of 0 min, 1 min, 5 min, 10 min, 15 min, and 20 min. All the measurements were carried out in a 100 μM DA solution in PBS 7.4, except for the incubation time study, which was conducted in a 10.0 μM DA solution in PBS 7.4. For all values $N = 3$.

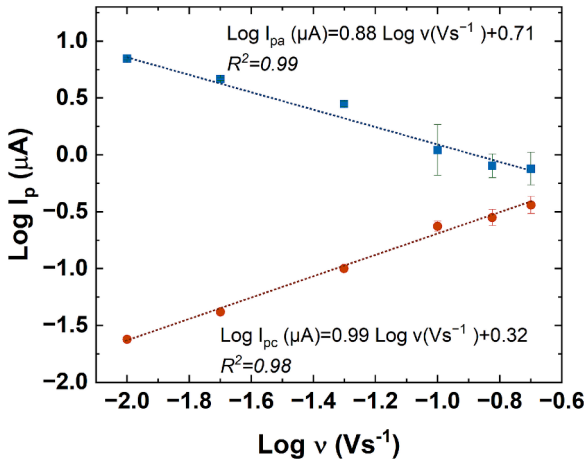

Fig. 8. Plot of the logarithm of anodic and cathodic peak currents vs. logarithm ν with fits of lines to these data and related equations. Effect of the scan rate was conducted in a 10.0 μM DA solution in PBS 7.4 at MIP/ta-C and the scan rate was varied considering the following values: 10.0 mVs^{-1}, 20.0 mVs^{-1}, 100 mVs^{-1}, 200 $mVs^{-1}$and mVs^{-1}.

evaluated by varying the pH of the electropolymerization solution (pHs 3.0, 4.0, 5.0, 6.0, 7.0, 8.0, and 9.0). After electropolymerization at each pH, the electrodes were subjected to a two-step washing process to remove the DA template molecules, followed by testing in a 100 μM DA PBS solution at pH 7.4 (physiologically relevant). The signal increased from pH 3.0 to 8.0, while it decreased at higher pH values, with the highest peak current observed at pH 8.0 (shown in Fig. 7B). The pH of the electropolymerization solution directly affects the formation of the molecular imprinted sites within the PPy matrix. At lower pH levels, the protonation of both DA and the PPy backbone leads to weaker interactions during the imprinting process, resulting in less efficient trapping of DA molecules and fewer well-defined imprinted sites. As the pH increases, the interaction between DA and the PPy network becomes more favorable, leading to better incorporation of DA within the polymer matrix and more efficient formation of accessible molecular imprinted sites. However, at higher pH levels (above 8.0), DA can be polymerized into polydopamine, which can hinder the removal of DA during the template removal step and reduce the accessibility of the imprinted sites for subsequent interaction with DA [30–32]. For this reason, pH 8.0 was determined to be optimal, as it strikes a balance between efficient molecular imprinting and ensuring that the imprinted sites remain accessible for DA detection after the washing process.

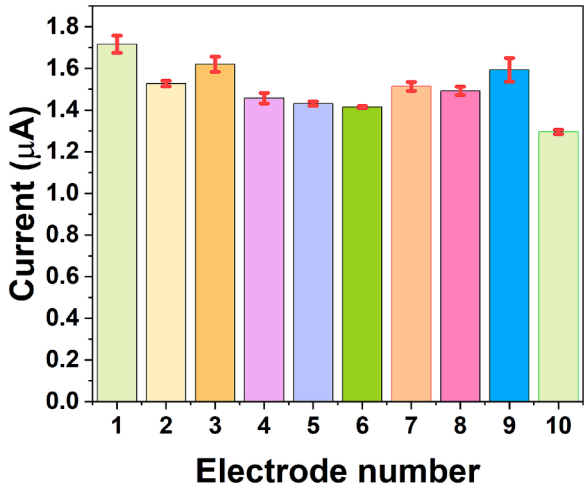

Fig. 9. Column plot showing the oxidation current for DA for different electrodes used in the same experimental conditions.

3.3.4. *Effect of the thickness of the MIP layer*

The thickness of the DA-imprinted PPy layer is proportional to the number of CV cycles utilized during the electropolymerization process. During the imprinting process, a variety of CV cycle numbers (5, 10, 15, and 20) were considered. The response signal of the produced MIP/ta-C electrodes in 100 μM DA PBS (pH 7.4) was then examined to determine the optimal thickness of the MIP layer at the ta-C electrode. Fig. 7C shows that increasing the thickness of the polymeric layer results in the development of a higher number of recognition sites, up to 10 cycles. However, if the film grows too thick, the template molecules remain stuck inside the PPy layer, making template removal difficult and limiting the number of accessible recognition sites. Thus, the optimal number of CV cycles was selected to be 10. Furthermore, the effect of the scan rate of CVs during the electropolymerization step was examined to determine the optimal performance. Lower potential scan rates promote the formation of a denser film, resulting in fewer available recognition sites. Conversely, higher scan rates yield a looser film, which also diminishes recognition capacity. Consequently, the optimal scan rate was identified to be 100 mV/s, as illustrated in Fig. S4.

3.3.5. *Effect of the incubation time*

The effect of the incubation time (ranging from 0 to 20 min) on the response signal of MIP/ta-C electrodes was studied in a 10.0 μM DA PBS (pH 7.4) solution. This incubation period provides DA molecules with sufficient time to interact with the imprinted recognition sites. The oxidation current significantly increased between 0 and 10 min of incubation time, while it saturated for times exceeding 10 min. This suggests that all active recognition sites were occupied within 10 min, as depicted in Fig. 7D.

The influence of the scan rate (ν) on the redox peak current of DA at the MIP/ta-C was investigated (Fig. 8). Both the anodic peak current (I_{pa}) and the cathodic peak current (I_{pc}) increased with the scan rate, ranging from 10.0 to 300 mVs^{-1}. Furthermore, there is a linear relationship between log I_p vs. log ν, with a slope approximately close to 1 as shown in Fig. 8, indicating an adsorption-controlled mechanism for the oxidation/reduction of DA on the MIP/ta-C electrode.

3.4. *Reproducibility and repeatability studies*

The reproducibility and repeatability of the MIP/ta-C electrodes toward DA detection were studied. Reproducibility was calculated qualitatively by studying the behavior of different electrodes under the same conditions. The standard deviation was generally found to be low among these electrodes, as shown in Fig. 9. Specifically, the standard deviation for 10 MIP/ta-C electrodes was calculated to be as low as 0.12 μA, which corresponds to a 7.90 % relative standard deviation. Repeatability was assessed by studying the behavior of the same electrode in the same conditions. The same electrode was used for DA detection several times, washing it electrochemically between different tests. Unfortunately, the performance of the electrode was found to decrease after the first use, as the response signal becomes lower. For this reason, an unused (new) MIP/ta-C electrode was used for each measurement.

3.5. *Analytical results*

The analytical performance of the MIP/ta-C electrodes was assessed across various DA concentrations (ranging from 0.10 to 1.00 μM) using

Table 5
Comparison of sensor performance of 15 nm ta-C based electrodes in PBS in our research group.

Electrode's material	Linear range (μM)	LOD (nM)	Sensitivity	E_{pa} (V) 100 μM DA	E_{pa} (V) 1 mM AA	References
ta-C (15 nm)	0.01–100	84.3	0.28	0.32	0.56	[15,23]
MIP/ta-C (15 nm)	**0.10–1.00**	**48.6**	**0.16**	**0.42**	**0.99**	**This work**

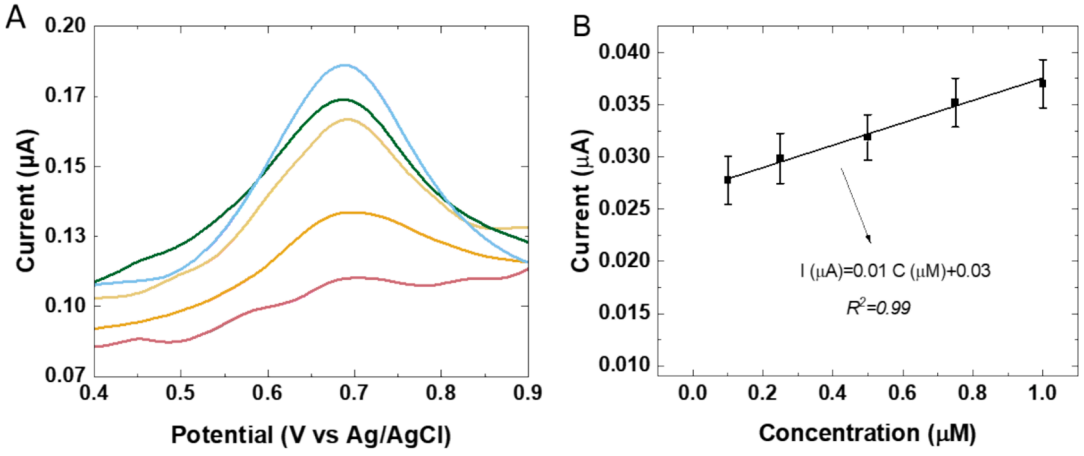

Fig. 10. (a) DPV signals for different concentrations of DA (100 nM, 250 nM, 500 nM, 750 nM and 1 μM) at MIP/ta-C electrode in 0.1 M PBS pH 7.4, and (b) The corresponding calibration plot under optimized conditions (N = 3). Fig. S2 shows the DPV of the MIP/ta-C electrode in PBS at pH 7.4.

Table 6
Comparison of the previous DA imprinted PPy electrochemical sensors.

Electrode's material	Linear range (μM)	Electrolyte	LOD (nM)	References
DA imprinted PPy /MWCNT/GAs[a]	0.005–20.0	PB (pH: 6)	1.67	[33]
DA imprinted PPy – o-PD[b]	–	PB (pH: 6)	3972	[3]
DA imprinted PPy/pThi/NPG[c]	0.30–100	PB (pH: 7)	100	[34]
DA imprinted poly (p-ATP)[d]	0.05–0.20	PBS (pH:7.4)	18.0	[1]
DA imprinted poly (AHQ) /GR[e]	0.10–1.40	PB (pH: 7)	32.0	[35]
DA imprinted Au/NGOQDs/NiS2/BC/MIP/GCE[f]	0.05–8.00 and 8.00–40.0	PBS (pH: 6.8)	2.80	[36]
DA imprinted ZnO NPs@C/3D-KSC integrated electrode [g]	0.00012–152	PBS (pH: 7)	0.04	[37]
DA imprinted FET Au gate electrode [h]	0.04–20.0	PBS (pH: 7.4)	96.0	[38]
DA imprinted PPy/ZnO nanotubes	0.02–5.00 & 10.0–800	$K_3(Fe(CN)_6)$	–	[39]
DA-aptamers and DA-imprinted PPy-modified AuNPs/rGO/GCE	0.05–10.0	PBS (pH: 7.4)	47.0	[40]
DA-imprinted o-phenylenediamine/NPGL/GCE [i]	2.00–180	PBS (pH: 7.0)	300	[41]
DA imprinted PPy /ta-C	**0.10–1.00**	**PBS (pH: 7.4)**	**48.6**	**This work**

[a] 3D-multi-walled carbon nanotube intercalated graphene aerogel; [b] o-phenylenediamine (o-PD); [c] polythionine (pThi), Nanoporous gold (NPG); [d] Poly(p-aminothiophenol) (p-ATP); [e] poly (5-amino 8-hydroxy quinoline) (poly (AHQ), reduced graphene oxide (GR); [f] AuNPs and nitrogen-doped graphene oxide quantum dots coated on NiS2/biomass carbon (Au/NGOQDs/NiS2/BC); [g] chitosan Film/Porous ZnO NPs@ carbon Nanospheres/Macroporous carbon (ZnO NPs@C/3D-KSC); [h] extended-gate field-effect transistor; [i] nanoporous gold leaf (NPGL).

DPV, chosen for its greater sensitivity compared to the CV method. DPV measurements were executed under optimized conditions in 0.10 M PBS at pH 7.4 as the supporting electrolyte (Fig. 10A). Notably, the response signal intensified with increasing DA concentration. Fig. 10B represents the calibration plot of the MIP/ta-C within the concentration ranges of 0.10 to 1.00 μM. The high correlation coefficient ($R^2 = 0.99$) for the calibration curve (depicted in Fig. 10B) underscores the robust linear relationship between DA concentration and peak current.

The sensitivity and LOD have been computed from the previously shown results and using Eqs. (2) and (3).

$$S = \frac{10 \cdot \delta}{m} \tag{2}$$

$$LOD = \frac{3 \cdot \delta}{m} \tag{3}$$

where σ is the standard deviation of the blank and m is the slope of the calibration curve. The sensitivity is calculated to be 162 nM, while the LOD was 48.6 nM for the slope of 0.01 μA/μM (in the range of 0.10 to 1.00 μM). The physiological concentration of DA is in the range of 5.00–700 nM, proving that the results obtained are physiologically relevant [22]. It is worth mentioning that unmodified ta-C electrodes are much less sensitive for DA sensing compared to the MIP/ta-C electrodes, as studied in our research group [15,23](refer to Table 5), which underlines the pivotal role of MIP in amplifying sensitivity. Additionally, the AA oxidation potential peak at MIP/ta-C shifted to more positive values compared to unmodified ta-C electrodes (refer to Table 5 and Fig. S5). Selectivity was not the focus of our study, as it has been previously investigated and reported by Rantataro et al. within our group [5]. Their findings indicated that AA does not consistently interfere with the electrochemical detection of DA in a cell culture medium. It is worth noting that AA experiences rapid degradation in the cell culture medium, with a half-life of 2.1 h, resulting in a 93.0 % decrease in concentration within 8 h and a 99.7 % decrease within 18 h. Consequently, AA becomes undetectable by electrodes over time, enabling effective monitoring of neurotransmitter concentration [5]. The MIP/ta-C sensor was tested in a 10.0 μM DA solution with serotonin (1.0 μM) and 3,4-dihydroxyphenylacetic acid (DOPAC, 10.0 μM) as potential interferences. The current signal variation remained minimal, within ± 5.1 %, demonstrating the sensor's reliable DA detection even in the presence of these structural analogues at physiological levels.

In comparison with the previous DA-imprinted PPy electrochemical sensors, the designed MIP/ta-C electrode demonstrated remarkable sensitivity for DA detection in physiologically relevant conditions at pH 7.4 in phosphate-buffered saline (PBS). Unlike many recently developed MIP-based DA sensors (refer to Table 6), our current study did not optimize the pH for DA testing, maintaining it at the physiological level (7.4) to achieve physiologically relevant sensitivity. This decision holds significance for *in vitro* studies and future applications involving cell culture media, serum, organ-on-a-chip systems, and beyond. Additional studies on electrochemical MIP-based sensors for various molecules are summarized in Table 7, highlighting target analytes, sensor performance, and electrolyte pH, positioning our work within broader advancements in the field.

4. Conclusions

The present work aims at the development of a sensitive MIP/ta-C/silicon-based electrochemical sensor for DA detection by combining the advantages of molecularly imprinting technology and ta-C/silicon-based electrodes. The ta-C thin films were successfully formed on the top silicon wafers by using a filtered cathodic vacuum arc system. The SEM, AFM, and Raman measurements indicated the formation of the MIP layer on the ta-C sample. Furthermore, electrochemical studies confirmed the high performance of MIP/ta-C compared to ta-C and NIP/ta-C toward DA sensing. All electrode fabrication steps were optimized for the detection of DA with physiologically relevant sensitivity in PBS (pH 7.4). The sensitivity was calculated to be 0.16 μA μM^{-1} cm^{-2}, while the LOD was 48.6 nM in the concentration range of 100 nM to 1.00 μM. The sensitivity was strongly improved compared to bare ta-C electrodes, bringing it down to the physiological range and making the device valuable for *in vitro* studies. Therefore, the methodology used was found

Table 7
Comparison of the previous MIP-based electrochemical sensors.

Electrode's material	Template molecule	Linear range (μM)	Electrolyte	LOD (nM)	References
Pefloxacin-imprinted PPy/BPNS[a]/AuNPs	Pefloxacin	0.005–10.0	PBS (pH: 2.5)	0.80	[42]
PBnPs[b]@cortisol-imprinted pyrrole/GnPs@CnFM/FCE	Cortisol	0.001–1.00	sweat	0.35	[43]
Norfloxacin-imprinted PPy/BPNS-AuNP/GCE	Norfloxacin	0.0001–10.0	PBS (pH: 5)	0.01	[44]
Norfloxacin-imprinted BP-PEDOT: PSS[c]/GCE	Norfloxacin	0.001–10.0	PBS (pH: 5.5)	0.25	[45]

[a] Black phosphorus nanocomposite (BPNS); [b] Prussian blue nanoparticles (PBnPs); [c] poly(3,4-ethylenedioxythiophene); polystyrene sulfonate-functionalized black phosphorene (BP-PEDOT:PSS);

to be effective in reaching the goals set. The sensor developed is fully compatible with current microsystems technologies and microelectrode arrays (MEAs) and can be easily integrated into a chip.

5. Declaration of generative AI in scientific writing

During the preparation of this work, the author(s) used ChatGPT 3.5 to improve readability and language. After using this tool/service, the author(s) reviewed and edited the content as needed and take(s) full responsibility for the content of the publication.

CRediT authorship contribution statement

Giorgia Rinaldi: Writing first draft – review & editing, Investigation, Formal analysis. **Khadijeh Nekoueian:** Investigation, Conceptualization, Validation, Formal analysis, Visualization, Writing – review & editing. **Jarkko Etula:** Resources, review & editing. **Tomi Laurila:** Supervision, Resources, Conceptualization, Writing – review & editing.

Declaration of competing interest

The authors declare that they have no known competing financial interests or personal relationships that could have appeared to influence the work reported in this paper.

Acknowledgements

The authors acknowledge Dr. Maedeh Akhoundian for AFM and Raman studies. This work was supported by funding from the European Union's Horizon2020 research project number 68011531 CONNECT. The authors acknowledge the provision of facilities by the Aalto University Ota Nano – Micronova Nanofabrication Center, OtaNano – Nanomicroscopy Center (Aalto-NMC).

Appendix A. Supplementary data

Supplementary data to this article can be found online at https://doi.org/10.1016/j.jelechem.2024.118742.

References

[1] N. Ermiş, N. Tinkiliç, Development of an electrochemical sensor for selective determination of dopamine based on molecularly imprinted poly(p-aminothiophenol) polymeric film, Electroanalysis 33 (2021) 1491–1501.
[2] N. Chauhan, S. Soni, P. Agrawal, Y.P.S. Balhara, U. Jain, Recent advancement in nanosensors for neurotransmitters detection: present and future perspective, Process Biochem. 91 (2020) 241–259.
[3] B. Si, E. Song, Molecularly imprinted polymers for the selective detection of multi-analyte neurotransmitters, Microelectron. Eng. 187 (2018) 58–65.
[4] S.E. Elugoke, A.S. Adekunle, O.E. Fayemi, E.D. Akpan, B.B. Mamba, E.-S.-M. Sherif, E.E. Ebenso, Molecularly imprinted polymers (MIPs) based electrochemical sensors for the determination of catecholamine neurotransmitters – review, Electrochem. Sci. Adv. 1 (2021) e2000026.
[5] S. Rantataro, L. Ferrer Pascual, T. Laurila, Ascorbic acid does not necessarily interfere with the electrochemical detection of dopamine, Sci. Rep. 12 (2022) 20225.
[6] M. Amiri, K. Nekoueian, R.S. Saberi, Graphene-family materials in electrochemical aptasensors, Anal. Bioanal. Chem. 413 (2021) 673–699.
[7] E. Leppänen, M. Akhoundian, S. Sainio, J. Etula, O. Pitkänen, T. Laurila, Structure-property relationships in carbon electrochemistry, Carbon 200 (2022) 375–389.
[8] T. Laurila, V. Protopopova, S. Rhode, S. Sainio, T. Palomäki, M. Moram, J.M. Feliu, J. Koskinen, New electrochemically improved tetrahedral amorphous carbon films for biological applications, Diam. Relat. Mater. 49 (2014) 62–71.
[9] T. Laurila, S. Sainio, M. Caro, Hybrid carbon based nanomaterials for electrochemical detection of biomolecules, Progress in Materials Science, Elsevier Ltd (2017) 499–594.
[10] E. Leppanen, A. Aarva, S. Sainio, M.A. Caro, T. Laurila, Connection between the physicochemical characteristics of amorphous carbon thin films and their electrochemical properties, J. Phys. Condens. Matter 33 (2021).
[11] J. Etula, N. Wester, S. Sainio, T. Laurila, J. Koskinen, Characterization and electrochemical properties of iron-doped tetrahedral amorphous carbon (ta-C) thin films, RSC Adv. 8 (2018) 26356–26363.
[12] S. Sainio, T. Palomäki, N. Tujunen, V. Protopopova, J. Koehne, K. Kordas, J. Koskinen, M. Meyyappan, T. Laurila, Integrated Carbon Nanostructures for Detection of Neurotransmitters, Mol. Neurobiol. 52 (2015) 859–866.
[13] S.E. Rodil, R. Olivares, H. Arzate, In vitro cytotoxicity of amorphous carbon films, Biomed. Mater. Eng. 15 (2005) 101–112.
[14] N. Wester, S. Sainio, T. Palomäki, D. Nordlund, V.K. Singh, L.-S. Johansson, J. Koskinen, T. Laurila, Partially reduced graphene oxide modified tetrahedral amorphous carbon thin-film electrodes as a platform for nanomolar detection of dopamine, J. Phys. Chem. C 121 (2017) 8153–8164.
[15] T. Palomäki, E. Peltola, S. Sainio, N. Wester, O. Pitkänen, K. Kordas, J. Koskinen, T. Laurila, Unmodified and multi-walled carbon nanotube modified tetrahedral amorphous carbon (ta-C) films as in vivo sensor materials for sensitive and selective detection of dopamine, Biosens. Bioelectron. 118 (2018) 23–30.
[16] S.A. Zaidi, Development of molecular imprinted polymers based strategies for the determination of dopamine, Sensors Actuators B: Chem., Elsevier B.V. (2018) 488–497.
[17] K. Nekoueian, M. Akhoundian, N. Wester, T. Laurila, An ultra-sensitive dopamine measurement platform based on molecularly imprinted polymer-carbon hybrid nanomaterials for in vitro use, Electrochim. Acta 445 (2023) 142029.
[18] K. Namsheer, C.S. Rout, Conducting polymers: a comprehensive review on recent advances in synthesis, properties and applications, RSC Adv. 11 (2021) 5659–5697.
[19] R. Ansari, Polypyrrole conducting electroactive polymers: synthesis and stability studies, J. Chem. 3 (2006) 186–201.
[20] J. Etula, N. Wester, T. Liljeström, S. Sainio, T. Palomäki, K. Arstila, T. Sajavaara, J. Koskinen, M.A. Caro, T. Laurila, What determines the electrochemical properties of nitrogenated amorphous carbon thin films? Chem. Mater. 33 (2021) 6813–6824.
[21] T. Palomäki, N. Wester, M.A. Caro, S. Sainio, V. Protopopova, J. Koskinen, T. Laurila, Electron transport determines the electrochemical properties of tetrahedral amorphous carbon (ta-C) thin films, Electrochim. Acta 225 (2017) 1–10.
[22] T. Palomäki, S. Chumillas, S. Sainio, V. Protopopova, M. Kauppila, J. Koskinen, V. Climent, J.M. Feliu, T. Laurila, Electrochemical reactions of catechol, methylcatechol and dopamine at tetrahedral amorphous carbon (ta-C) thin film electrodes, Diam. Relat. Mater. 59 (2015) 30–39.
[23] T. Palomäki, E. Peltola, S. Sainio, N. Wester, O. Pitkänen, K. Kordas, J. Koskinen, T. Laurila, Corrigendum to "Unmodified and multi-walled carbon nanotube modified tetrahedral amorphous carbon (ta-C) films as in vivo sensor materials for sensitive and selective detection of dopamine" (Biosensors and Bioelectronics, 118 (23–30), (S0956566318305190) (10.1016/j.bios.2018.07.018)), Biosensors Bioelectron., Elsevier Ltd 2019 (2018) 281–284.
[24] N. Leibl, L. Duma, C. Gonzato, K. Haupt, Polydopamine-based molecularly imprinted thin films for electro-chemical sensing of nitro-explosives in aqueous solutions, Bioelectrochemistry 135 (2020) 107541.
[25] T.-P. Chen, T. Liu, T.-L. Su, J. Liang, Self-polymerization of dopamine in acidic environments without oxygen, Langmuir 33 (2017) 5863–5871.
[26] A.J. Bard, L.R. Faulkner, H.S. White, Electrochemical methods: fundamentals and applications, John Wiley & Sons, 2022.
[27] V. Protopopova, A. Iyer, N. Wester, A. Kondrateva, S. Sainio, T. Palomäki, T. Laurila, M. Mishin, J. Koskinen, Ultrathin undoped tetrahedral amorphous carbon films: the role of the underlying titanium layer on the electronic structure, Diam. Relat. Mater. 57 (2015) 43–52.
[28] V.S. Protopopova, N. Wester, M.A. Caro, P.G. Gabdullin, T. Palomäki, T. Laurila, J. Koskinen, Ultrathin undoped tetrahedral amorphous carbon films: thickness dependence of the electronic structure and implications for their electrochemical behaviour, PCCP 17 (2015) 9020–9031.
[29] R. McCann, S. Roy, P. Papakonstantinou, G. Abbas, J. McLaughlin, The effect of thickness and arc current on the structural properties of FCVA synthesised ta-C and ta-C: N films, Diam. Relat. Mater. 14 (2005) 983–988.
[30] C. Malitesta, E. Mazzotta, R.A. Picca, A. Poma, I. Chianella, S.A. Piletsky, MIP sensors – the electrochemical approach, Anal. Bioanal. Chem. 402 (2012) 1827–1846.
[31] V. Suryanarayanan, C.-T. Wu, K.-C. Ho, Molecularly imprinted electrochemical sensors, Electroanalysis 22 (2010) 1795–1811.
[32] Y. Liu, K. Ai, L. Lu, Polydopamine and Its derivative materials: synthesis and promising applications in energy, environmental, and biomedical fields, Chem. Rev. 114 (2014) 5057–5115.
[33] X. Ma, F. Gao, R. Dai, G. Liu, Y. Zhang, L. Lu, Y. Yu, Novel electrochemical sensing platform based on a molecularly imprinted polymer-decorated 3D-multi-walled carbon nanotube intercalated graphene aerogel for selective and sensitive detection of dopamine, Anal. Methods 12 (2020) 1845–1851.
[34] J. Yang, Y. Hu, Y. Li, Molecularly imprinted polymer-decorated signal on-off ratiometric electrochemical sensor for selective and robust dopamine detection, Biosens. Bioelectron. 135 (2019) 224–230.
[35] V.M.A. Mohanan, A.K. Kunnummal, V.M.N. Biju, Selective electrochemical detection of dopamine based on molecularly imprinted poly (5-amino 8-hydroxy quinoline) immobilized reduced graphene oxide, J. Mater. Sci. 53 (2018) 10627–10639.
[36] Z. Lu, Y. Li, T. Liu, G. Wang, M. Sun, Y. Jiang, H. He, Y. Wang, P. Zou, X. Wang, A dual-template imprinted polymer electrochemical sensor based on AuNPs and nitrogen-doped graphene oxide quantum dots coated on NiS2/biomass carbon for simultaneous determination of dopamine and chlorpromazine, Chem. Eng. J. 389 (2020) 124417.
[37] Y. Song, J. Han, L. Xu, L. Miao, C. Peng, L. Wang, A dopamine-imprinted chitosan Film/Porous ZnO NPs@ carbon Nanospheres/Macroporous carbon for electrochemical sensing dopamine, Sens. Actuators B 298 (2019) 126949.

[38] T. Kajisa, W. Li, T. Michinobu, T. Sakata, Well-designed dopamine-imprinted polymer interface for selective and quantitative dopamine detection among catecholamines using a potentiometric biosensor, Biosens. Bioelectron. 117 (2018) 810–817.
[39] H.-H. Wang, X.-J. Chen, W.-T. Li, W.-H. Zhou, X.-C. Guo, W.-Y. Kang, D.-X. Kou, Z.-J. Zhou, Y.-N. Meng, Q.-W. Tian, S.-X. Wu, ZnO nanotubes supported molecularly imprinted polymers arrays as sensing materials for electrochemical detection of dopamine, Talanta 176 (2018) 573–581.
[40] M. Shen, X. Kan, Aptamer and molecularly imprinted polymer: Synergistic recognition and sensing of dopamine, Electrochim. Acta 367 (2021) 137433.
[41] N. Li, C. Nan, X. Mei, Y. Sun, H. Feng, Y. Li, Electrochemical sensor based on dual-template molecularly imprinted polymer and nanoporous gold leaf modified electrode for simultaneous determination of dopamine and uric acid, Microchim. Acta 187 (2020) 496.
[42] G. Li, X. Qi, J. Wu, X. Wan, T. Wang, Y. Liu, Y. Chen, Y. Xia, Highly stable electrochemical sensing platform for the selective determination of pefloxacin in food samples based on a molecularly imprinted-polymer-coated gold nanoparticle/black phosphorus nanocomposite, Food Chem. 436 (2024) 137753.
[43] X. Mei, J. Yang, X. Yu, Z. Peng, G. Zhang, Y. Li, Wearable molecularly imprinted electrochemical sensor with integrated nanofiber-based microfluidic chip for in situ monitoring of cortisol in sweat, Sens. Actuators B 381 (2023) 133451.
[44] G. Li, X. Qi, J. Wu, L. Xu, X. Wan, Y. Liu, Y. Chen, Q. Li, Ultrasensitive, label-free voltammetric determination of norfloxacin based on molecularly imprinted polymers and Au nanoparticle-functionalized black phosphorus nanosheet nanocomposite, J. Hazard. Mater. 436 (2022) 129107.
[45] G. Li, J. Wu, X. Qi, X. Wan, Y. Liu, Y. Chen, L. Xu, Molecularly imprinted polypyrrole film-coated poly(3,4-ethylenedioxythiophene):polystyrene sulfonate-functionalized black phosphorene for the selective and robust detection of norfloxacin, Mater. Today Chem. 26 (2022) 101043.